Title
DYNAMICS OF ANGULAR MOMENTUM ACXULULATION IN DAMPED NUCLEAR REACTIONS

Authors
Randrup, J.
Dossing, T.

Publication Date
1984-05-01

Lawrence Berkeley Laboratory
UNIVERSITY OF CALIFORNIA

Presented at the Conference on Theoretical Approaches of Heavy Ion Reaction Mechanisms, Paris, France, May 14-18, 1984; and to be published in Nuclear Physics A

DYNAMICS OF ANGULAR MOMENTUM ACCUMULATION IN DAMPED NUCLEAR REACTIONS

J. Randrup and T. Døssing

May 1984

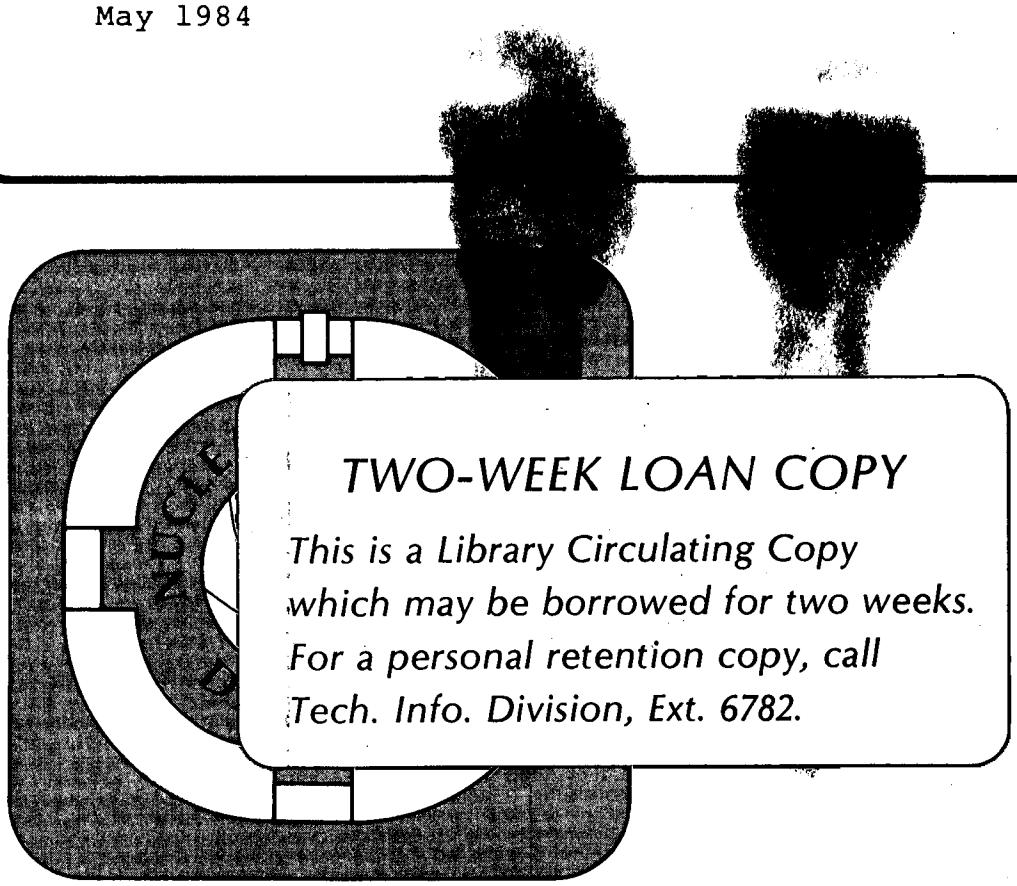

Prepared for the U.S. Department of Energy under Contract DE-AC03-76SF00098

DISCLAIMER

DYNAMICS OF ANGULAR MOMENTUM ACCUMULATION IN DAMPED NUCLEAR REACTIONS*

Jørgen Randrup and Thomas Døssing+

Nuclear Science Division, Lawrence Berkeley Laboratory,
University of California, Berkeley, California 94720

The dynamical evolution of the correlated angular momentum distribution in a damped nuclear reaction is discussed within the framework of the nucleon exchange transport model.

1. INTRODUCTION

The accumulation of angular momentum in a damped nuclear reaction is an important topic for our understanding of low-energy nuclear dynamics. The fragment spins carry considerable information about the reaction dynamics: while the mass and charge distribution can be characterized by two mean values and three covariances, the correlated spin distribution requires two mean values and thirteen non-trivial covariances. On the other hand, the spin-related observables are more difficult to extract experimentally.

The present contribution reports briefly on some selected results of a recent study of the dynamical evolution of angular momentum in damped nuclear reactions.[1,2] The study is carried out within the framework of the nucleon exchange transport model,[3] in which the dissipation of the macroscopic variables is caused by the inelastic interactions of individual nucleons with the time-dependent mean field. In the case of a binary system, as is temporarily created during a damped reaction, this one-body mechanism appears as a "window" dissipation caused by the transfer of nucleons between the two reaction partners, in addition to a "wall" friction caused by the reflection of nucleons from the changing potential in the interaction zone between the two nucleides.

The reacting system is idealized as two spherical nucleides A and B. The relative orbital angular momentum is $\vec{L} = \vec{R} \times \vec{P}$ where $\vec{R}$ is the relative position and $\vec{P}$ is the relative momentum. The associated moment of inertia is $\mathcal{I}_R = \mu R^2$. The angular momenta, or spins, of the individual nucleides are $\vec{S}^A$ and $\vec{S}^B$, and $\mathcal{I}_A$ and $\mathcal{I}_B$ are the associated moments of inertia. Specific details about this model can be found in Appendix A of ref[4].

---

*This work was supported by the Director, Office of Energy Research, Division of Nuclear Physics of the Office of High Energy and Nuclear Physics of the U.S. Department of Energy under Contract DE-AC03-76SF00098.

+Niels Bohr Fellow, granted by the Royal Danish Academy of Science.

2. EQUATIONS OF MOTION

In ref.[3], the mobility tensors relating to the two fragment spins $\vec{S}^A$ and $\vec{S}^B$ were found to be

$$\begin{aligned} \overleftrightarrow{M}^{AA} &= mN\,(a^2\,\overleftrightarrow{T} + c_{ave}^2\,\overleftrightarrow{I}) \\ \overleftrightarrow{M}^{AB} &= mN\,(ab\,\overleftrightarrow{T} - c_{ave}^2\,\overleftrightarrow{I}) = \overleftrightarrow{M}^{BA} \\ \overleftrightarrow{M}^{BB} &= mN\,(b^2\,\overleftrightarrow{T} - c_{ave}^2\,\overleftrightarrow{I}) \end{aligned} \tag{1}$$

Here $\overleftrightarrow{I}$ is the identity tensor and $\overleftrightarrow{T} = \overleftrightarrow{I} - \hat{R}\hat{R}$ projects onto the plane perpendicular to the dinuclear axis R. The distances to the "window" plane from the two nuclear centers are denoted by a and b, with a + b = R, while c_{ave} is the average off-axis displacement of the transferred nucleons. The nucleon mass is denoted m, and N is the overall form factor governing the rate of nucleon transfer between the two nucleides A and B.

In addition to the fragment spins $\vec{S}^A$ and $\vec{S}^B$, it is also necessary to consider the evolution of the orbital angular momentum $\vec{L}$. This is because we wish to use a coordinate system whose direction fluctuates with respect to an external inertial system (and hence the components of the total angular momentum $\vec{J}$ will fluctuate). It is notationally convenient to denote any of the angular-momentum labels A, B, L by the letters F, G, ... so that $\vec{S}^F = \vec{S}^A, \vec{S}^B, \vec{L}$ for F = A, B, L, respectively. The mobility tensor relating to the orbital angular momentum can then be obtained by exploiting the conservation of the total angular momentum $\vec{J} = \vec{S}^A + \vec{S}^B + \vec{L}$.

In terms of the mobility coefficients the spin transport coefficients are given as follows. The diffusion coefficients are simply the corresponding mobility coefficients multiplied by the "effective temperature" τ^*: $D^{FG} = M^{FG}\tau^*$. The drift coefficients are obtained by multiplying the mobility tensor with the corresponding generalized forces, i.e., minus the rotational frequencies $\vec{\omega}^F = \vec{S}^F/\mathcal{I}_F$: $\vec{V}^F = -\sum_G \overleftrightarrow{M}^{FG}\cdot\vec{\omega}^G = -\sum_G \overleftrightarrow{M}^{FG}\cdot\vec{S}^G/\mathcal{I}_G$. Here and in the following the sum over the labels G extends over G = A, B, L.

In order to take full account of the so called tilting mode, it is necessary to employ a "body-aligned" orthonormal reference system. Specifically, we define the coordinate system xyz: $\hat{z} = \hat{R}$, $\hat{y} = \hat{L}$, $\hat{x} = \hat{y} \times \hat{z}$. The choice of $\hat{z} = \hat{R}$ ensures that the mobility tensors $\overleftrightarrow{M}^{FG}$ are diagonal in the spatial indices. Since $\hat{y} = \hat{L}$, the orbital angular momentum $\vec{L}$ has only components in the y-direction. We need then consider the temporal evolution of S_x^A, S_y^A, S_z^A, S_x^B, S_y^B, S_z^B, L_y. In a standard collision experiment, all are initially zero except for L_y which equals the total angular momentum J. It follows from the symmetry of the

problem that the mean values $\langle S_x^F \rangle$ and $\langle S_z^F \rangle$ and also the covariances σ_{xy}^{FG} and σ_{yz}^{FG} will remain zero throughout the reaction.

The equations of motion for the non-vanishing mean values and covariances are given by

$$
\begin{aligned}
\dot{S}_y^F &= \sum_G \left(M_t^{FG} S_y^G + \frac{1}{L_y}\sigma_{xx}^{FG} M_t^{GL}\right)/\mathcal{I}_G + \frac{\tau^*}{L_y}\left(2M_t^{FL} - \frac{S_y^F}{L_y} M_t^{LL}\right) \\
\dot{\sigma}_{xx}^{FH} &= 2\tau^* M_t^{FH} - \sum_G \left(\sigma_{xx}^{FG} M_t^{GH} + M_t^{FG}\sigma_{xx}^{GH}\right)/\mathcal{I}_G - \omega_R\left(\sigma_{xz}^{FH} + \sigma_{zx}^{FH}\right) \\
&\quad - \frac{S_y^F}{L_y}\left(2\tau^* M_t^{LH} - \sum_G M_t^{LG}\sigma_{xx}^{GH}/\mathcal{I}_G\right) - \left(2\tau^* M_t^{FL} - \sum_G \sigma_{xx}^{FG} M_t^{GL}/\mathcal{I}_G\right)\frac{S_y^H}{L_y} \\
&\quad + 2\tau^* \frac{S_y^F}{L_y} M_t^{LL} \frac{S_y^H}{L_y} \\
\dot{\sigma}_{yy}^{FH} &= 2\tau^* M_t^{FH} - \sum_G \left(\sigma_{yy}^{FG} M_t^{GH} + M_t^{FG}\sigma_{yy}^{GH}\right)/\mathcal{I}_G \\
\dot{\sigma}_{zz}^{FH} &= 2\tau^* M_n^{FH} - \sum_G \left(\sigma_{zz}^{FG} M_n^{GH} + M_n^{FG}\sigma_{zz}^{GH}\right)/\mathcal{I}_G - \omega_R\left(\sigma_{xz}^{FH} + \sigma_{zx}^{FH}\right) \\
\dot{\sigma}_{xz}^{FH} &= -\sum_G \left(\sigma_{xz}^{FG} M_n^{GH} + M_t^{FG}\sigma_{xz}^{GH}\right)/\mathcal{I}_G - \omega_R\left(\sigma_{xx}^{FH} - \sigma_{zz}^{FH}\right) + 2\tau^* \frac{S_y^F}{L_y} M_t^{LG}\sigma_{xz}^{GH}/\mathcal{I}_G
\end{aligned}
\tag{2}
$$

Here we have omitted the bracket around the mean values of S_y^F for notational simplicity, since confusion can hardly arise.

In the above equation for the mean value the first term is the drift coefficient. In the equations for the covariances, the first term is the diffusion coefficient (which vanishes for the non-diagonal components) while the subsequent term represents the restoring term acting to saturate the growth of σ. The terms containing ω_R arise from the orbital rotation which continually mixes the in-plane components. The remaining terms contain $\langle L_y \rangle$ in the denominator and arise from the transformation to the fluctuating coordinate system aligned with $\vec{L}$. These terms are derived under the standard assumption that all spin dispersions are small in comparison with $\langle L_y \rangle$. While this is only well satisfied for larger impact parameters, the equations do remain well-behaved for more central collisions (which contribute only a small part of the reaction cross section) and even for head-on reactions the solutions are correct to within 25%. Although these latter terms are of the corrective type, they are essential in ensuring the proper long-time behavior of the solutions, namely an approach towards statistical equilibrium.

In the preceding we have referred the spin moments to a coordinate system defined in terms of the instantaneous values of $\hat{R}$ and $\hat{L}$. However, the direction $\hat{L}$ can not be determined in a collision experiment, so it is necessary to

transform the results to a coordinate system which can be externally defined. In a collision experiment two directions are readily determined: the beam direction $\hat{t}$ and the asymptotic dinuclear direction $\hat{R}(\infty)$. In terms of these two directions we define the following external coordinate system XYZ: $\hat{Z} = \hat{R}$, $\hat{Y} = \hat{R} \times \hat{t}$, $\hat{X} = \hat{Y} \times \hat{Z}$. Since the internal and the external coordinate systems have the same z-axis, the two are related by a rotation around the z-axis, $\mathcal{R}_z(\zeta)$. Since the distribution of the angle ζ between the directions L and Y is determined by the in-plane spin variances, the transformation from xyz to XYZ can be made.

The resulting spin distribution corresponds to a definite impact parameter, given by the specified value of the total angular momentum J. The model also yields equations of motion for the kinetic energy loss and its covariance with the spin variables. Therefore, it is possible to obtain an "observable" spin distribution gated by energy loss rather than impact parameter.

3. EQUILIBRIUM

In the preceding we have outlined how the dynamical evolution of the dinuclear spins can be calculated. The results of such calculations can best be understood in terms of the appropriate equilibrium solutions and the associated relaxation times.

In analogy with the treatment of the two-particle problem, we introduce the following spins and associated moments of inertia,

$$\begin{aligned} \vec{S} &= \vec{S}^A + \vec{S}^B \quad , & \mathcal{I}_+ &= \mathcal{I}_A + \mathcal{I}_B \\ \vec{S}^- &= \mathcal{I}_-\left(\frac{\vec{S}^A}{\mathcal{I}_A} - \frac{\vec{S}^B}{\mathcal{I}_B}\right) \quad , & \mathcal{I}_- &= \frac{\mathcal{I}_A \mathcal{I}_B}{\mathcal{I}_A + \mathcal{I}_B} \end{aligned} \tag{3}$$

They are analogous to the total and relative motion, respectively. For a given total angular momentum J, and under the standard assumption that the variances are small compared to $\langle L_y \rangle^2$, it is straightforward (albeit tedious) to demonstrate that the dynamical spin equations (2) have a unique stationary solution given by

$$\begin{aligned} \langle L_y \rangle &= \frac{\mathcal{I}_R}{\mathcal{I}_0} J \quad , & \overleftrightarrow{\sigma}^{LL} &= \tau^* \mathcal{I}_+ \frac{\mathcal{I}_R}{\mathcal{I}_0} \hat{y}\hat{y} \\ \langle S_y^+ \rangle &= \frac{\mathcal{I}_+}{\mathcal{I}_0} J - \tau^* \mathcal{I}_+ \frac{\mathcal{I}_0}{\mathcal{I}_R} \frac{1}{J} \quad , & \overleftrightarrow{\sigma}^{++} &= \tau^* \mathcal{I}_+ \frac{\mathcal{I}_0}{\mathcal{I}_R} (\hat{x}\hat{x} + \hat{z}\hat{z}) + \tau^* \mathcal{I}_+ \frac{\mathcal{I}_R}{\mathcal{I}_0} \hat{y}\hat{y} \\ \langle S_y^- \rangle &= 0 \quad , & \overleftrightarrow{\sigma}^{--} &= \tau^* \mathcal{I}_- \overleftrightarrow{I} \end{aligned} \tag{4}$$

where we have included terms to the first order in the effective temperature

τ^*. During the reaction, the moments of the spin distribution will at each instant evolve towards these equilibrium values, which in turn vary in time due to the time dependence of the relative moment of inertia $\mathcal{I}_R$ and the effective temperature τ^*. Below we shall first discuss the stationary solution in terms of a statistical model, and next we shall discuss the time scales for the approach towards equilibrium.

The part of the macroscopic hamiltonian $\mathcal{H}$ containing the angular-momentum variables in the disphere is

$$\mathcal{H}_{rot} = \frac{\vec{S}^{A2}}{2\mathcal{I}_A} + \frac{\vec{S}^{B2}}{2\mathcal{I}_B} + \frac{\vec{L}^2}{2\mathcal{I}_R} \tag{5}$$

For a given value of $\vec{J} = \vec{S}^A + \vec{S}^B + \vec{L}$, the lowest-energy mode of rotational motion in the disphere is a rigid rotation with each of the three angular momenta given by $\vec{S}^F = \mathcal{I}_F\vec{J}/\mathcal{I}_0$ where $\mathcal{I}_0 = \mathcal{I}_A + \mathcal{I}_B + \mathcal{I}_R$. Relative to this yrast mode of motion, intrinsic rotational excitations are possible. These excitations carry no net angular momentum and can be classified in two groups according to whether the two spheres turn in the same or in the opposite sense, i.e., a purely positive mode has $\vec{S}^- = \vec{0}$ and a purely negative mode has $\vec{S}^+ = \vec{0}$, where $\vec{S}^+$ and $\vec{S}^-$ are given in Eq. (3).

We first consider the problem using the coordinate system x'y'z' defined by $\hat{z}' = \hat{R}$, $\hat{y}' = \hat{I}$, $\hat{x}' = \hat{y}' \times \hat{z}'$, where $\vec{I} = \vec{J} - \vec{J}\cdot\hat{R}\,\hat{R}$ is the projection of the total angular momentum $\vec{J}$ on the plane perpendicular to $\vec{R}$. In order to bring the rotational hamiltonian (5) on normal form we introduce the following auxiliary spin variable $\vec{s} = \vec{S}^+ - (\mathcal{I}_+/\mathcal{I}_0)J_{y'}\hat{y}'$. This transformation has unit jacobian since $\hat{y}'$ is independent of $\vec{S}^+$ and we obtain

$$\begin{aligned}\mathcal{H}_{rot} &= \frac{1}{2\mathcal{I}_A}\left(\frac{\mathcal{I}_A}{\mathcal{I}_+}\vec{S}^+ + \vec{S}^-\right)^2 + \frac{1}{2\mathcal{I}_B}\left(\frac{\mathcal{I}_B}{\mathcal{I}_+}\vec{S}^+ - \vec{S}^-\right)^2 + \frac{1}{2\mathcal{I}_R}(\vec{J} - \vec{S}^+)^2 \\ &= \frac{J^2}{2\mathcal{I}_0} + \frac{1}{2\mathcal{I}_+}\frac{\mathcal{I}_0}{\mathcal{I}_R}(s_{x'}^2 + s_{y'}^2) + \frac{1}{2\mathcal{I}_+}\frac{\mathcal{I}_R}{\mathcal{I}_0}s_{z'}^2 + \frac{\vec{S}^{-2}}{2\mathcal{I}_-}\end{aligned} \tag{6}$$

Here the first term represents the yrast energy associated with a rigid rotation while the additional terms arise from the six normal modes of intrinsic rotational excitation of the disphere. The first of these terms is the energy of the two degenerate *wriggling* modes, where the two spheres rotate in the same sense around an axis perpendicular to $\hat{R}$. The next term is associated with the *tilting* mode arising when $\vec{J}$ has a component along the dinuclear axis $\hat{R}$; the two spheres thus turn in the same sense around $\hat{R}$. These three are the positive modes. The last term arises from the three degenerate negative modes: the *twisting* mode, where the two spheres rotate oppositely around $\vec{R}$, and the two *bending* modes, where the spheres turn oppositely around an axis

perpendicular to $\vec{R}$.

Assume now that the rotational modes are weakly coupled to the remainder of the system, which is considered as a heat reservoir with the temperature τ. When $\tau << J^2/2\,\mathcal{I}_0$, the six normal rotational modes are approximately harmonic. It is then possible to show that the ensuing thermal equilibrium distribution is characterized by

$$\langle S^F_{y'} \rangle = \frac{\mathcal{I}_F}{\mathcal{I}_0} J - \frac{\mathcal{I}_F \mathcal{I}_+}{\mathcal{I}_R} \frac{\tau}{2J}$$

$$\sigma^{FG}_{y'y'} = \sigma^{FG}_{x'x'} = \left(\frac{\mathcal{I}_R}{\mathcal{I}_0} \mathcal{I}_F \mathcal{I}_G + \epsilon_{FG}\, \mathcal{I}_A \mathcal{I}_B \right) \frac{\tau}{\mathcal{I}_A + \mathcal{I}_B} \tag{7}$$

$$\sigma^{FG}_{z'z'} = \left(\frac{\mathcal{I}_0}{\mathcal{I}_R} \mathcal{I}_F \mathcal{I}_G + \epsilon_{FG}\, \mathcal{I}_A \mathcal{I}_B \right) \frac{\tau}{\mathcal{I}_A + \mathcal{I}_B}$$

(The symbol ϵ_{FG} is one when F = G and minus one otherwise.) This result is in accordance with the analysis by Moretto.[5]

The above result was expressed in the I-aligned coordinate system x'y'z'. A transformation to our standard "body-fixed" L-aligned system xyz yields the following equilibrium distribution

$$\langle S^F_y \rangle = \frac{\mathcal{I}_F}{\mathcal{I}_0} J - \frac{\mathcal{I}_F \mathcal{I}_0}{\mathcal{I}_R} \frac{\tau}{J}$$

$$\sigma^{FG}_{yy} = \left(\frac{\mathcal{I}_R}{\mathcal{I}_0} \mathcal{I}_F \mathcal{I}_G + \epsilon_{FG}\, \mathcal{I}_A \mathcal{I}_B \right) \frac{\tau}{\mathcal{I}_A + \mathcal{I}_B} \tag{8}$$

$$\sigma^{FG}_{zz} = \sigma^{FG}_{xx} = \left(\frac{\mathcal{I}_0}{\mathcal{I}_R} \mathcal{I}_F \mathcal{I}_G + \epsilon_{FG}\, \mathcal{I}_A \mathcal{I}_B \right) \frac{\tau}{\mathcal{I}_A + \mathcal{I}_B}$$

This result is identical to the stationary solution (4) of the dynamical equations (2).

In the variances in (7) and (8) the first terms arise from the positive modes (wriggling and tilting) while the second terms arise from the isotropic negative modes (bending and twisting). The most pronounced effect of the transformation from x'y'z' to xyz is the increase in the in-plane wriggling variance σ^{++}_{xx} by the factor $(\mathcal{I}_0/\mathcal{I}_R)^2 \cong 2$ so that the isotropy in the plane perpendicular to $\vec{R}$ is replaced by isotropy in the plane perpendicular to $\vec{L}$. A different normal form of the rotational hamiltonian (5) for an asymmetrical disphere has been introduced by Schmitt and Pacheco.[6] This leads to different definitions of the wriggling and bending modes, but the result expressed in the original variables, eq. (7), is of course the same.

4. EVOLUTION IN A SYMMETRIC DISPHERE

In Section 3 we introduced the spins $\vec{S}^{++}$ and $\vec{S}^{--}$; they are particularly convenient variables when the two spheres are equal. In the symmetric case, where a = b and $\mathcal{I}_A = \mathcal{I}_B$, the mixed mobility tensor $\overleftrightarrow{M}^{+-}$ vanishes so that the dynamical equations for $\vec{S}^{--}$ decouple from the rest; furthermore, the mobility tensor $\overleftrightarrow{M}^{--}$ is isotropic.

Typical time scales for the approach to equilibrium can be obtained by dividing the asymptotic values by the respective initial time derivatives. This yields for the transversal spin components σ_{xx}^{++} and σ_{yy}^{++} the time scales $\frac{\mathcal{I}_o}{\mathcal{I}_R} t_{++}$ and $\frac{\mathcal{I}_R}{\mathcal{I}_o} t_{++}$, respectively, where

$$t_{++} = \frac{\tau^* \mathcal{I}_+}{2\tau^* M^{LL}} = \frac{\mathcal{I}_+}{2mNR^2} \tag{9}$$

while for the components of $\overleftrightarrow{\sigma}^{--}$ we find

$$t_{--} = \frac{\tau^* \mathcal{I}_-}{2\tau^* M^{--}} = \frac{\mathcal{I}_-}{2mNc_{ave}^2} \tag{10}$$

Thus, $t_{++}/t_{--} = (c_{ave}^2/R^2) << 1$.

Solving the equations more rigorously for the idealized case of constant coefficients, the time development of the variances are governed by these relaxation times, for example:

$$\overleftrightarrow{\sigma}^{--} = \mathcal{I}_{-\tau}^* \left[1 - e^{-t/t_{--}}\right] \overleftrightarrow{I} \tag{11}$$

The normal variance σ_{zz}^{++} does not receive contributions directly through the transfer process, but only indirectly by the orbital rotation of σ_{xx}^{++} via σ_{xz}^{++}. Solving the equations for these variances, the relaxation time for σ_{xx}^{++} is t_{++}, which we already discussed, while for σ_{zz}^{++} the typical time scale is

$$t_{+z} \cong \left(4\omega_R^2 \frac{L_y}{J_y} t_{++}\right)^{-1} , \tag{12}$$

which is usually fairly long.

The time scales for the evolution of mean values are approximately twice the ones relevant for the variances:

$$S_y^+ = \frac{\mathcal{I}_+}{\mathcal{I}_o}\left[1 - e^{-\frac{\mathcal{I}_o}{\mathcal{I}_R}\frac{t}{2t_{++}}}\right] , \quad S_y^- = 0 \tag{13}$$

5. ILLUSTRATIVE RESULTS

In the preceeding section we have discussed the characteristic features of the spin evolution with an emphasis on the qualitative aspects. We now wish to illustrate the theory quantitatively by making applications to one reaction of actual experimental interest, namely 1400 MeV ^{165}Ho + ^{165}Ho. A pictorial impression of the evolution of the dinuclear geometry can be gained from Fig. 1.

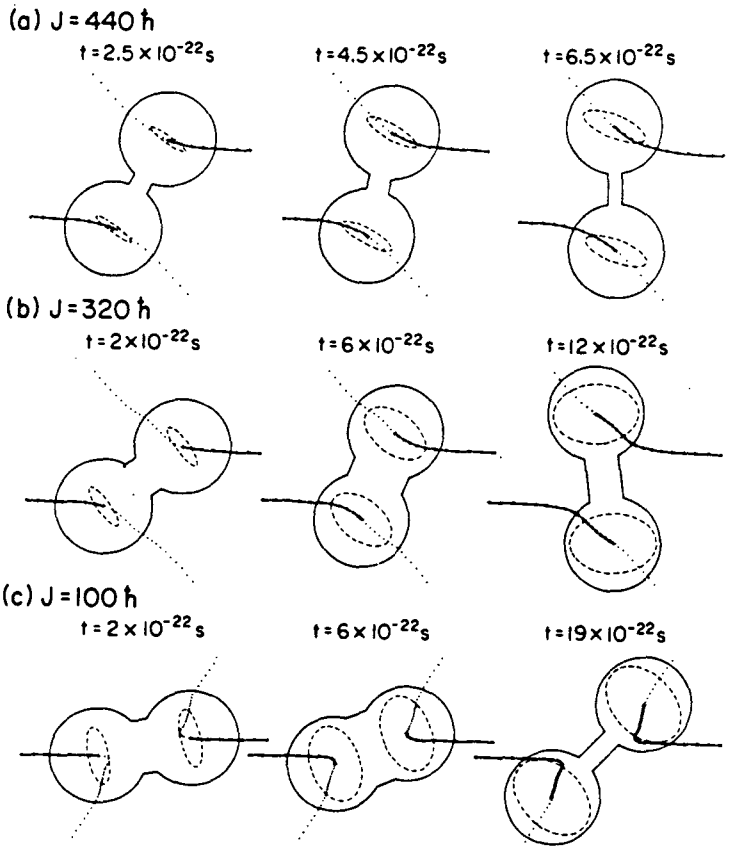

FIGURE 1

For three different values of the total angular momentum J, the dinuclear complex produced in the reaction 1400 MeV ^{165}Ho + ^{165}Ho is shown at three different points in time: shortly after the neck has opened, at the time of closest approach, and right before the neck collapses. (The actual times indicated are measured from the time of the nuclei approach to a surface separation of s = 4 fm.) The dots indicate past and future locations of the nuclear centers at intervals of 10^{-22} sec. The dashed ellipses indicate the one-sigma contours of the in-plane distribution of the nuclear angular momenta $\vec{S}^A$ and $\vec{S}^B$ scaled so that one fm corresponds to two ħ (the nuclear radii are 6.3 fm).

We now consider in some detail the calculated dynamical evolution of the angular momenta during the reaction phase. First, we consider the various relaxation times introduced in Section 4. They are shown in Fig. 2 as functions of time, for a number of different values of the total angular momentum J. We note that throughout the reaction phase the relaxation times t_{++} associated with the two wriggling modes are considerably shorter than t_{--} associated with the negative modes, as already expected since $c^2_{ave} << R^2$. The relaxation time for the tilting mode is fairly long but has an opposite behavior, both as a function of time and in its dependence on J. By comparing the relaxation times with the reaction times it is possible to obtain an expectation for how far the various modes will evolve towards equilibrium. Thus, for not too large impact parameters, we expect the wriggling modes to achieve nearly complete relaxation, contrary to the negative modes for which this is at most expected for the smallest impact parameters. The tilting mode is generally expected to acquire little excitation.

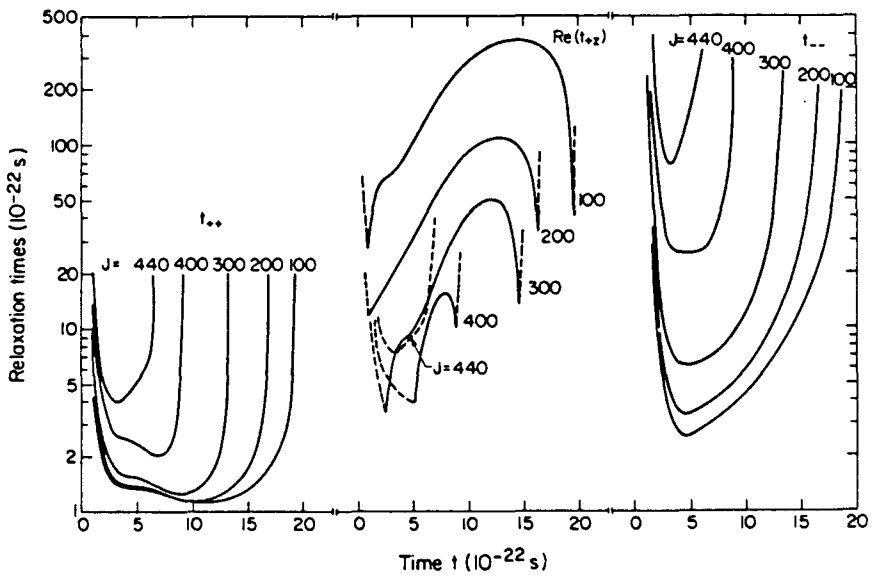

FIGURE 2
Calculated local relaxation times for the reaction 1400 MeV ^{165}Ho + ^{165}Ho for various values of the total angular momentum J. The relaxation times for the two positive perpendicular modes (wriggling) are denoted t_{++}, while that for the positive longitudinal mode (tilting) is denoted t_{+z}. The relaxation time for the three negative modes (bending and twisting) is denoted t_{--}.

The calculated dynamical evolution of the mean fragment spin projection is shown in Fig. 3, for three selected J-values. For the highest value, J = 440 ħ, the reaction is over before the equilibrium mean value can be reached. For the intermediate value, J = 320 ħ, the equilibrium value is nearly achieved around the time of closest approach. This equilibrium mean spin decreases as the two fragments recede and the relative moment of inertia grows. Therefore, the mean spin exhibits a maximum as a function of time. The same is true at the most central reaction, J = 100 ħ, but here the equilibrium values are of course smaller.

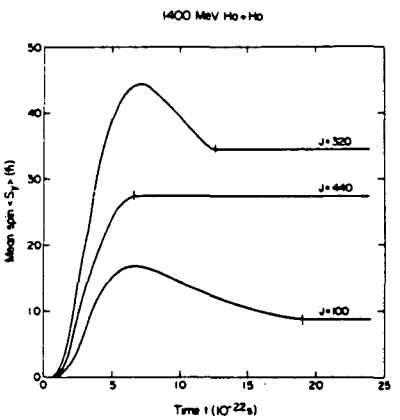

FIGURE 3
Calculated time evolution of the mean fragment spin $\langle S_y \rangle$ in the reaction 1400 MeV ^{165}Ho + ^{165}Ho for various values of the total angular momentum J. The neck snapping, after which the spins remain constant, is indicated by a small vertical bar.

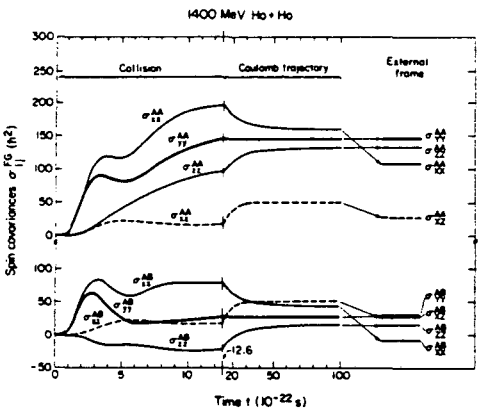

FIGURE 4
Calculated time evolution of the various spin covariances σ_{ij}^{FG} in the reaction 1400 MeV ^{165}Ho + ^{165}Ho for a total angular momentum of J = 320 ħ. At the time of neck snapping ($t = 12.6 \cdot 10^{-22}$s) the time scale is changed by a factor of ten. After the asymptotic values have been reached, the effect of transforming to the external reference frame from XYZ is shown.

The calculated spin covariances are displayed in Fig. 4 as functions of time. The figure has three parts. The first shows the dynamical evolution during the reaction phase. It is clearly seen how σ_{xx}^{FG} and σ_{yy}^{FG} increase rapidly at early times; this is a reflection of the fast wriggling relaxation time (see Fig. 2). The local bumps in σ_{xx}^{FG} and σ_{yy}^{FG} around the time of closest approach ($t \approx 3 \cdot 10^{-22}$ s) are caused by a minimum in the effective temperature τ^*. [The effective temperature is initially nearly proportional to

the relative nuclear velocity and hence at first it decreases. Later on, when the relative motion has subsided, τ^* is close to the intrinsic temperature τ which increases in time. Thus τ^* exhibits a minimum which occurs approximately at the turning point of the relative motion.] The evolution of σ_{zz}^{FG} is considerably slower, as expected from Fig. 2. Most of σ_{zz}^{FG} is associated with the negative twisting mode as evidenced by the fact that the covariance σ_{zz}^{AB} is negative, but, as the difference between σ_{zz}^{AA} and σ_{zz}^{AB} indicates, there is also a fair amount of tilting. The second part of the figure shows, on a condensed time scale, the rotation of the covariances along the exit Coulomb trajectory. Finally, the third part shows the result of transforming to the external coordinate system XYZ. This transformation is seen to have a substantial effect on the x-components; in fact σ_{xx}^{AB} becomes negative.

The equiprobability contours of the fragment spin distribution are ellipsoids whose common shape and orientation are determined by the appropriate covariances. In order to given a visual impression of the spin evolution we have included in Fig. 1 contours of the spin distribution projected onto the xz-plane. One notes how the fairly peripheral collision ($J = 440\ \hbar$) inhibits the build-up of negative spin modes so the distribution is very elongated. Furthermore, the smallness of the form factor prevents the distribution from aligning itself relative to the dinuclear axis. For $J = 320\ \hbar$ the window grows wider and the isotropic negative modes are more readily excited; the distribution also follows better the turning dinuclear axis. These features are even more apparent for $J = 100\ \hbar$.

6. COMPARISON TO EXPERIMENT

At present, our information about angular momentum in damped nuclear reactions arises from three types of observable: the multiplicity of γ-rays, the circular polarization of γ-rays, and the angular correlation between the direction of motion of a reaction product and a sequential ejectile. In the present study we do not address the polarization data since they are yet fairly crude with respect to the dependence on energy loss.

The γ-multiplicity data gives information about the distribution of the total magnitude of fragment spin. When the spin dispersions are relatively small, we may obtain approximate expressions for the spin magnitude moments by expanding around the mean spin $\langle \vec{S}^F \rangle$. The leading order terms in the spin magnitude moments are the moments of the spin distribution along the reaction normal, so mainly the distribution along the reaction normal is probed in γ-multiplicity experiments.

The γ-emission is preceded by neutron evaporation which modifies the spin distribution. This effect is taken carefully into account in our calculations.

In Fig. 5 we show spin magnitude moments extracted from two sets of data on γ-multiplicities[7,8] together with our calculated results. For the small TKEL, the calculated mean value of the spin is rising too steeply by a factor of two, relative to the experimental results. For the higher TKEL, the experimental values first reach a maximum and then decrease slightly towards the highest TKEL. The theoretical results reproduce these features and the maximum has approximately the correct size, but it is reached at a too small TKEL, and the decrease for the highest TKEL is too pronounced.

The variances are in good agreement with the data. About 40% of the calculated variance is due to the correlation between the spins in the nuclei, especially the appreciable positive covariance $\sigma_{\gamma\gamma}^{AB}$ along the reaction normal. The presence of this correlation explains in a natural way the rather large variance of the sum of spin magnitudes seen in the γ-multiplicity data.

The average spin magnitude provides information about the relative importance of different types of friction acting in the relative motion of the two nuclei during a collision. Our results indicate that the ratio between the radial and tangential friction, as obtained with the present implementation of the nucleon exchange model, is too small.

For given impact parameter, the variance of the spin along the reaction normal is just given by the accumulated variance along the intrinsic y-direction. The variances along this direction increase rapidly when the nuclei come into contact, and are dominated by the positive wriggling mode. However, the subsequent integration over impact parameters to obtain TKEL gated distributions also contributes substantial variances and positive covariances so that the resulting dispersions become less sensitive to the specific model.

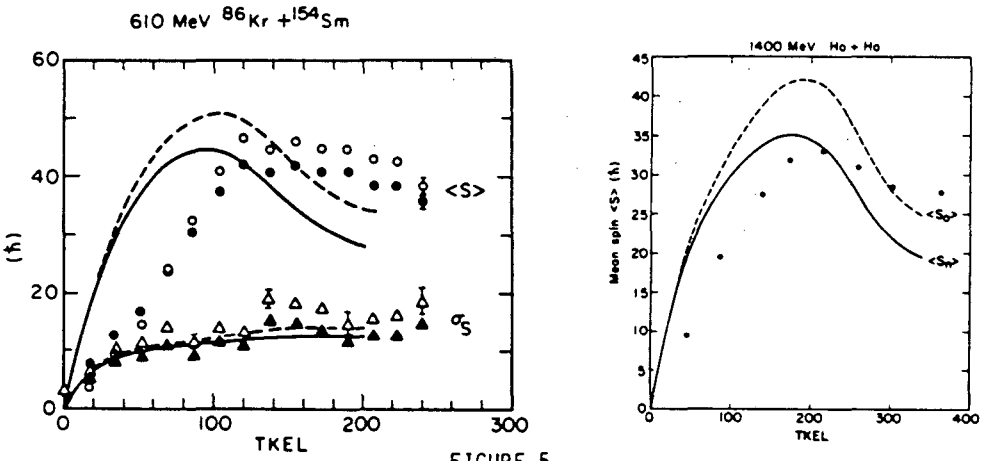

FIGURE 5
Calculated and measured[7,8] values of the mean spin magnitude and the associated covariance before (dashed) and after (solid) neutron evaporation.

Angular correlation data gives information about the distribution of the spin directions. The moments of the directional distribution are the statistical spherical tensors. The tensor of rank two is the most important, giving the *alignment* along the reaction normal $P_{YY} = \langle(3S_Y^2 - S^2)/2S^2\rangle$ and the *asymmetry* between the in-plane components $P_{XZ} = \langle(S_X^2 - S_Z^2)/S^2\rangle$. Thus, angular correlation experiments mainly probe the in-plane variances of the spin distribution in one nucleus, but only relative to the magnitude of the spin.

For a definite value of the spin magnitude in one of the reaction products, the terms of order zero and two of the angular correlation of sequential decay products emitted from that nucleus yield

$$4\pi\omega(\theta,\phi) = 1 + B_2(S)P_{YY}(S)P_2(\cos\theta) + \frac{3}{4} B_2(S)P_{XZ}(S)\sin^2\theta\cos\phi \quad . \tag{14}$$

Here the coordinate system has the polar axis along the reaction normal and diagonalizes the in-plane spin variance tensor. P_2 is the second order Legendre polynomial and $B_2(S)$ is the second order angular distribution coefficient for the given kind of decay. For fission and for large spins $S > 3K_o$ we have approximately $B_2(S) \cong 5(3K_o^2 - S^2)/2S^2$, where K_o is the familiar parameter giving the dispersion of the distribution of K quantum numbers of the saddle shape.

The tensor elements $P_{YY}(S)$ and $P_{XZ}(S)$ as well as the angular distribution coefficients and the fission probability vary with the spin magnitude S. In our actual calculations we include also fourth order terms and integrate over spin magnitude, taking into account competition between fission and neutron emission at all steps in a neutron decay cascade.

Figure 6 shows the experimental[9] and calculated in-plane angular correlation for three different kinetic energy losses for each of the two reactions Kr + Bi and Kr + U. The calculation agrees well with the data regarding the position of the extrema of the in-plane angular correlation, along the principal axes of the spin variance tensor. [Only for TKEL = 170 MeV in the Kr + Bi reaction do we get a discrepancy here, but this TKEL is in the calculation located at the upper edge of the energy loss distribution and is not focussed in scattering angle, so the discrepancy is not so serious.] The amplitude of the calculated variation is too small relative to the data by a factor of two. However, it should be kept in mind here that two other data sets for similar reactions with Bi or Pb disagree with the data shown on Fig. 6: one[10] displays in-plane anisotropies of approximately the same magnitude as calculated; and the other[11] shows almost no in-plane variation.

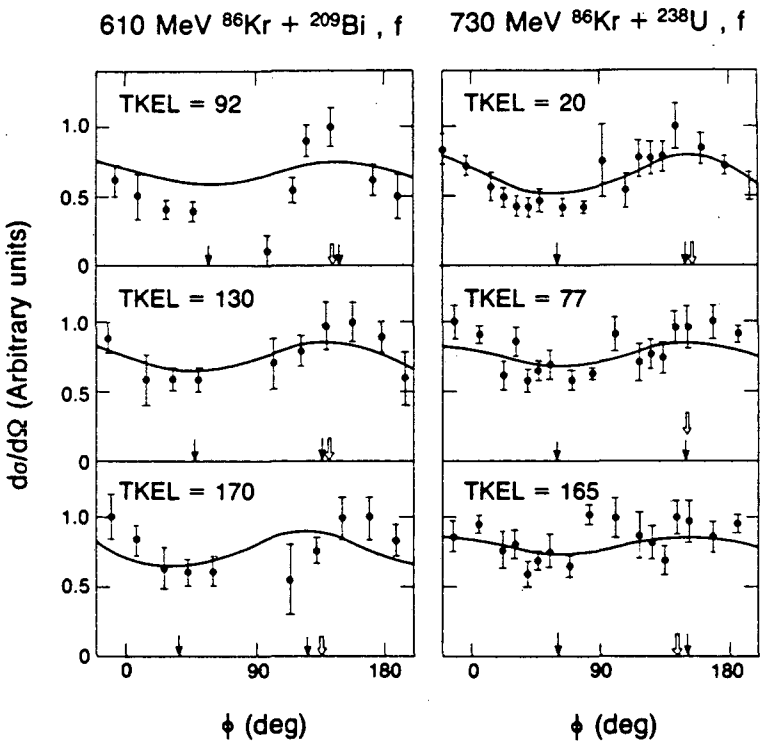

FIGURE 6
Calculated and measured[9] angular correlation in the reaction plane for fission of the heavy nucleus produced in the reactions 610 MeV ^{86}Kr + ^{209}Bi and 730 MeV ^{86}Kr + ^{238}U. $\phi = 90^{\circ}$ corresponds to the beam axis. The open arrow for each TKEL shows the target recoil direction in the lab-frame and the solid arrows point to the directions of principal axes of the in-plane components of the spin variance tensor.

The location of the maximum close to the average direction of the dinuclear axis during the reaction supports our result that the relaxation times for spin variances along the axis are longer than the reaction time and longer than the relaxation times for the spin variances perpendicular to the axis.

7. CONCLUDING REMARKS

The nucleon exchange transport model has addressed a variety of observables in damped nuclear reactions. The mass and charge distributions appear to be well described by the model,[12] and also the division of the excitation energy among the two fragments is in good accordance with data.[13] We have refined the model considerably in order to achieve a detailed description of the angular momentum accumulation,[1] and have also developed the treatment of the subse-

quent decay processes in order to calculate observed quantities.[2] Spin-related data obtained by different probes can then be confronted in a unified manner.

Our comparisons with data have yielded good agreement for a number of features, but the mean spin magnitude appears to increase too rapidly with energy loss, suggesting the presence of an additional radial dissipation. Further studies are required to clarify whether this shortcoming is a consequence of the simple classical calculation of the transport coefficients or signals the action of a different damping mechanism.

On rather general grounds, the present model predicts specific correlations between the two fragment spins. The spin spin correlations contain valuable novel information about the reaction dynamics and their experimental determination offers the field an exciting new prospect.

REFERENCES

1) T. Døssing and J. Randrup, LBL-16825 (1983).

2) T. Døssing and J. Randrup, LBL-16826 (1983).

3) J. Randrup, Nucl. Phys. A327 (1979) 490.

4) J. Randrup, Nucl. Phys. A383 (1983) 468.

5) L.G. Moretto and R.P. Schmitt, Phys. Rev. C21 (1980) 204.

6) R.P. Schmitt and A.J. Pacheco, Nucl. Phys. A379 (1982) 313.

7) P.R. Christensen, O. Hansen, O. Nathan, F. Videbaek, H. Freiesleben, H., C. Britt and S.H. van der Werf, Nucl. Phys. A390 (1982) 336.

8) R.J. McDonald, A.J. Pacheco, G.J. Wozniak, H.H. Bolotin, L.G. Moretto, C. Schuck, S. Shih, R.M. Diamond and F.S. Stephens, Nucl. Phys. A373 (1982) 54.

9) P. Dyer, R.J. Puigh, R. Vandenbosch, T.D. Thomas, M.S. Zisman and L. Nunnelly, Nucl. Phys. A322 (1979) 205;
R.J. Puigh, P. Dyer, R. Vandenbosch, T.D. Thomas, L. Nunnelly and M.S. Zisman, Phys. Lett. 86B (1979) 24;
R. Vandenbosch (1983) private communication.

10) D. von Harrach, P. Glassel, Y. Civelekoglu, R. Manner and H.J. Specht, Phys. Rev. Lett. 42 (1979) 1728.

11) C. Le Brun, J.F. Lecolley, F. Lefebures, M. L'Haridon, A. Osmont, J.P. Patry and J.C. Steckmeyer, in Proc. XX Int. Winter Meeting on Nucl. Phys., Bormio, Italy, January 1982 (University of Milano, 1982).

12) W.U. Schroder et al., Phys. Lett. 98B (1981) 355;
H.C. Britt et al., Phys. Rev. C26 (1982) 1999.

13) R. Vandenbosch, Workshop on Nuclear Dynamics III, 5-9 March 1984, Copper Mountain, Colorado.

TECHNICAL INFORMATION DEPARTMENT
LAWRENCE BERKELEY LABORATORY
UNIVERSITY OF CALIFORNIA
BERKELEY, CALIFORNIA 94720